Hindawi Publishing Corporation
Journal of Nanomaterials
Volume 2016, Article ID 7825456, 11 pages
http://dx.doi.org/10.1155/2016/7825456

Research Article

The Optimum Fabrication Condition of p-Type Antimony Tin Oxide Thin Films Prepared by DC Magnetron Sputtering

Huu Phuc Dang,[1] Quang Ho Luc,[2] Tran Le,[3] and Van Hieu Le[4]

[1]*Industrial University of HCMC, Ho Chi Minh City 700000, Vietnam*
[2]*Faculty of Foundation Sciences, HCMC University of Technology and Education, Ho Chi Minh City 700000, Vietnam*
[3]*Faculty of Physics and Engineering Physics, University of Sciences, VNU-HCMC, Ho Chi Minh City 700000, Vietnam*
[4]*Faculty of Material Sciences, University of Sciences, VNU-HCMC, Ho Chi Minh City 700000, Vietnam*

Correspondence should be addressed to Tran Le; ltran@hcmus.edu.vn

Received 14 March 2016; Accepted 8 May 2016

Academic Editor: Zhaoyao Zhan

Transparent Sb-doped tin oxide (ATO) thin films were fabricated on quartz glass substrates via a mixed (SnO_2 + Sb_2O_3) ceramic target using direct current (DC) magnetron sputtering in ambient Ar gas at a working pressure of 2×10^{-3} torr. X-ray diffraction (XRD), X-ray photoelectron spectroscopy (XPS), Hall-effect, and UV-vis spectra measurements were performed to characterize the deposited films. The substrate temperature of the films was investigated in two ways: (1) films were annealed in Ar ambient gas after being deposited at room temperature or (2) they were deposited directly at different temperatures. The first process for fabricating the ATO films was found to be easier than the second process. The deposited films showed p-type electrical properties, a polycrystalline tetragonal rutile structure, and their average transmittance was greater than 80% in the visible light range at the optimum annealing temperature of 500°C. The best electrical properties of the film were obtained on a 10 wt% Sb_2O_3-doped SnO_2 target with a resistivity, hole concentration, and Hall mobility of 0.55 Ω·cm, 1.2×10^{19} cm^{-3}, and 0.54 $cm^2V^{-1}s^{-1}$, respectively.

1. Introduction

Optoelectronic devices are found in many areas of society, from simple household appliances and multimedia systems to communications, optical monitoring, and medical instruments. The majority of optoelectronic devices are LEDs, laser diodes, photodiodes, and solar cells. Transparent conducting oxides (TCOs), which required as electrodes in these above optoelectronic devices, are made of Sn-doped In_2O_3 (ITO) [1], Al-doped ZnO (AZO) [2], Ga-doped ZnO (GZO) [3], Sb-doped SnO_2 (ATO) [4], or F-doped SnO_2 (FTO) [5], which have low resistivities (10^{-3}–10^{-4} Ω·cm) and high transparencies (80–90%). However, research on p-type TCOs has only recently begun.

The first candidate is p-type delafossite; $CuY_{1-x}Ca_xO_2$, $CuScO_{2+x}$, $CuCr_{1-x}Mg_xO_2$, and $CuScO_2$, as well as $AgFeO_2$ [6–11] …, have low resistivities but a present limitation in stability and have low transparencies, narrow band gaps, and difficult compositions. The second candidate is ZnO; however, it is difficult to produce p-type ZnO due to self-compensation effects [12–14]. Compared with ZnO, SnO_2 is a wide band gap semiconductor (3.6–4 eV) [15, 16] with good chemical, mechanical, and thermal stabilities [17–19]. Additionally, tin can easily be doped by group III metals because tin has a valence of 4.

Recently, the p-type doping of SnO_2 thin films was studied using metal elements in group III. For example, Al [20, 21] and Ga [22] have been incorporated into the structure as the acceptor impurities. Later, Ji et al. [23] and Ni et al. [24] also obtained p-type SnO_2 thin films doping In and Sb. Besides, Ni et al. [25] found that the incorporation of group IIA atoms (Zn) was also suitable for doping SnO_2, and Mao et al. [26] reported an In-Ga codoping method to realize p-type SnO_2 thin films with a high mobility.

The previous research has been focused on thin films synthesized by RF magnetron sputtering [20, 22, 24–30], the sol-gel [31, 32], spay-pyrolysis [33], or PLD [34]. Among these deposition methods, RF magnetron sputtering method is widely used because of high deposition rate, good adhesion, and easy control of the electrical properties of the films

by controlling processing parameters such as sputtering power, pressure, and temperature, particularly postannealing temperatures. However, no report explained clearly how to achieve the p-type by annealing and why thin films were not directly prepared with the various temperatures as well as why the thin films were deposited at 200°C after postannealing. The results of the previous research have not yet solved this problem, and, furthermore, a DC magnetron sputtering process has not yet been studied. Because the ionic radius of the Sb^{3+} ion (0.76 Å) is similar to that of Sn^{4+} (0.71 Å), we studied optical, electrical properties and the crystal structure of Sb-doped SnO_2 films deposited on quartz substrates by DC magnetron sputtering from ceramic targets made of a mixture of SnO_2 and Sb_2O_3. The parameters investigated were the substrate temperature during fabrication, the annealing temperature, and the percentage of the Sb_2O_3 dopant.

2. Experimental Techniques

SnO_2:Sb (ATO) thin films were deposited on quartz substrates from a ceramic target composed of a mixture of (SnO_2 + Sb_2O_3) by DC magnetron sputtering in ambient Ar gas at a working pressure of 2×10^{-3} torr with the Sb_2O_3 (wt%) varying from 0% to 15%, on a Univex 450 system. The quartz glass substrates were ultrasonically cleaned in 10% NaOH/acetone/deionized water solution for 35 min. Before deposition, the target was presputtered for 15 min to remove any contaminants on the target surface. The sputtering power and the target to sample distance were 15 W and 7 cm, respectively.

The substrate temperature of the films was investigated in two ways: (1) the films were deposited directly at different temperatures from room temperature to 500°C and heating and cooling rate 20°C/min, respectively, and (2) they were annealed in ambient Ar gas after being deposited at room temperature with the same heating and cooling rate as part 1.

The thicknesses of the thin films were measured using the SCOUT program by fitting the modeled spectrum to the experimental spectrum. By the controlling the deposition time, the thickness of SnO_2 and ATO films were about 400 nm. The structure of the ATO films was studied using an X-ray diffractometer (D8 ADVANCE) operated at 40 kV and 40 mA with Cu–Kα radiation. The optical transmittance was measured in the wavelength range 200–1100 nm using a UV-vis Jasco V-530. The film resistivity was measured at room temperature using the four-point probe method. A Hall measurement system (HMS 3000), which operated at room temperature, was used to measure the carrier concentration and the mobility. X-ray photoelectron spectroscopy (XPS) was measured at room temperature on an ESCALAB and the *I-V* characteristics were measured using a semiconductor testing system (Keithley 2400).

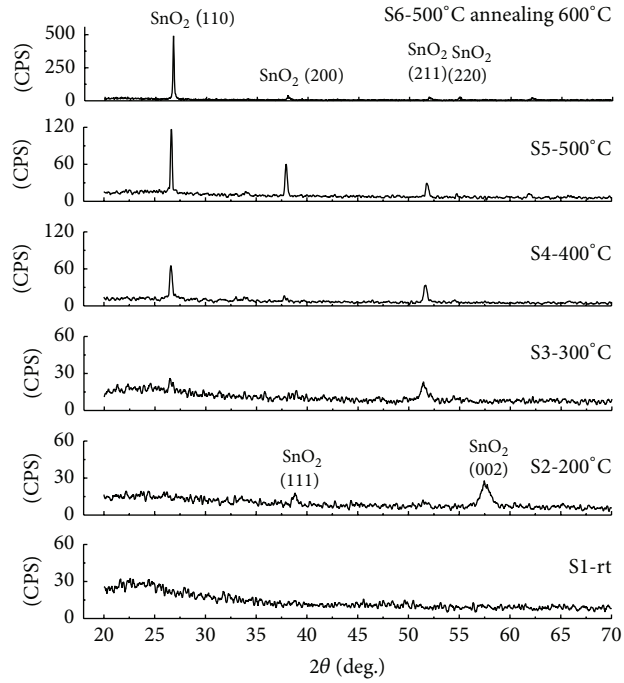

Figure 1: The X-ray diffraction patterns of SnO_2 films deposited at different temperatures.

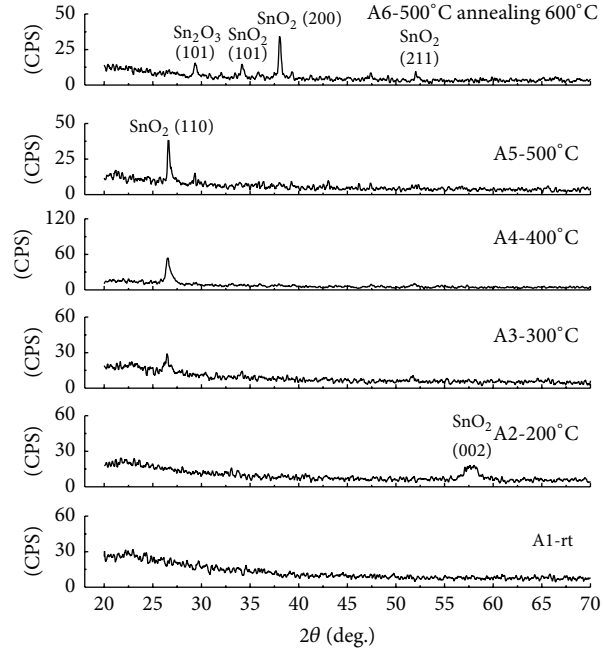

Figure 2: The X-ray diffraction patterns of ATO films deposited at different temperatures.

3. Results and Discussion

3.1. Structural Properties. Figures 1 and 2 show the XRD patterns of the SnO_2 and the ATO films (15% ATO films deposited from ATO target with 15% wt Sb_2O_3) deposited directly on quartz substrates at different temperatures. In particular, the temperature was applied directly to the films during the fabrication process; however, S6 and A6 films were deposited at 500°C followed by annealing at 600°C because the evaporation rate from substrates is greater than the condensation rate on substrates at temperatures above 500°C. Figure 1 shows that all films made at room temperature had an amorphous structure; the films started to crystallize

at 200°C with a SnO_2 tetragonal rutile structure (JCPDS Number 41-14445). The films had better crystalline quality at approximately 400°C marked by the appearance of the (110) peak, and the intensity of the peak sharply increased for the films deposited at 500°C and annealed at 600°C. Figure 2 shows that ATO films started to crystallize at 200°C with a SnO_2 tetragonal rutile structure and no peaks from antimony or antimony oxide phases appear in the XRD patterns, indicating that antimony could be incorporated into the tin oxide lattice. Several authors also showed all SnO_2 films doping atoms such as Ta [35], In-Ga [26], Sb [24, 34], Ga [22], Zn [28], and In [31] are in rutile phase without any secondary phases of dopant atoms or their oxides, indicating the incorporation of dopants into host lattice. Figure 2 also shows that there is the appearance of Sn_2O_3 phase (101) for films deposited at 500°C and the films deposited at 500°C followed by annealing at 600°C had one more Sn_2O_3 phase ($\bar{2}30$). In particular, the SnO_2 phase (110) disappeared and phase (101) appeared for ATO 500°C followed by annealing 600°C while it contrasted to SnO_2 films. This could also be the substitution of Sn^{4+} by Sb^{3+}. In fact, the report [36, 37] had also the same results that the (110) surface transformed to (101) surface which is rich in Sn^{2+} atoms (i.e., rich oxygen vacancy) as Sn^{4+} were substituted by Sn^{2+}.

The above results indicate that the ATO films can be made p-type through the annealing step after deposition at room temperature. Therefore, to avoid evaporating the material on the substrate, which occurs when the film is deposited at a higher temperature, the film can be deposited at room temperature and then annealed at various temperatures.

The XRD patterns of the as-deposited SnO_2 thin films and those annealed below 550°C are shown in Figure 3. The films become polycrystalline and are in the rutile phase with (110), (101), and (211) orientations. When the SnO_2 films were annealed at 550°C and 600°C, the Sn_2O_3 phase appeared and can contribute to the positive carriers, which result in the p-type films. It shows clearly in electrical properties (Table 2).

Figure 4 shows that the peak intensity of the ATO films is lower than those of the SnO_2 films under the same conditions, indicating that the dopant Sb^{3+} ions could replace the Sn^{4+} ions sites. When annealed above 500°C, the Sb^{3+} are activated to substitute Sn^{4+} significantly and there is appearance of Sn_2O_3 phase which is not recorded at SnO_2 films of the same fabricated conditions. The energy released from the replacement of Sn^{4+} by Sb^{3+} also contributes to the oxygenation of Sn_2O_3 to SnO_2 when annealed at 600°C. This oxygenation does not occur at SnO_2 films of the same fabricated conditions. The ATO films have lower resistivities (Table 2) with the presence of the Sn_2O_3 phase at an annealing temperature of 550°C. However, to confirm whether the positive contribution of Sn^{3+} is significant, the ATO films were annealed for 2 hours.

Figure 5 shows that the reflection intensity for (110), (101), and (211) increased versus annealing time, showing the high crystalline nature of the ATO films. Sn_2O_3 phase (101) disappeared at 500°C and appeared at 600°C for 2 h compare to 1 h. Besides, ATO annealed at 550°C for 2 h had one more Sn_2O_3 phase being (030). All transformation from Sn_2O_3 phase to SnO_2 phase and vice versa could be the attribution to films energy released from the substitution of Sn^{4+} by Sb^{3+} as mentioned in the discussion of Figure 4. Next, we investigated the effect of the doping percentage on the structure of the ATO films.

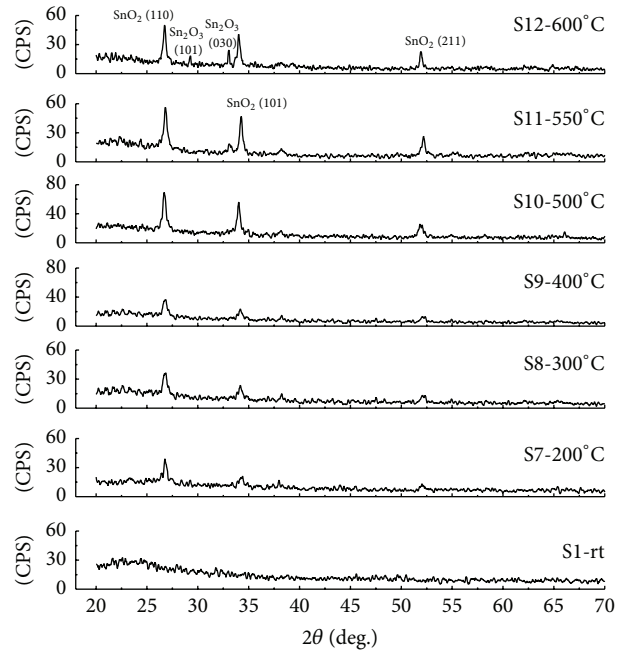

Figure 3: The X-ray diffraction patterns of SnO_2 films annealed at different temperatures for 1 h after being deposited at room temperature.

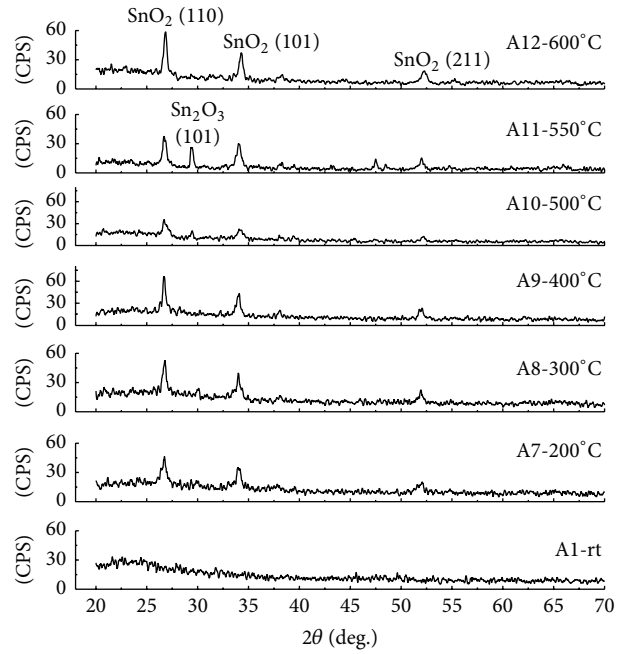

Figure 4: The X-ray diffraction patterns of 15% ATO films annealed at different temperatures for 1 h after being deposited at room temperature.

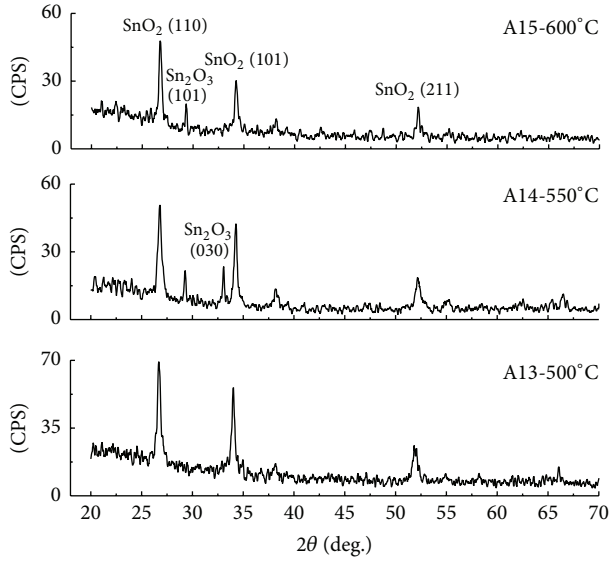

Figure 5: The X-ray diffraction patterns of 15% ATO films annealed at different temperatures for 2 h after being deposited at room temperature.

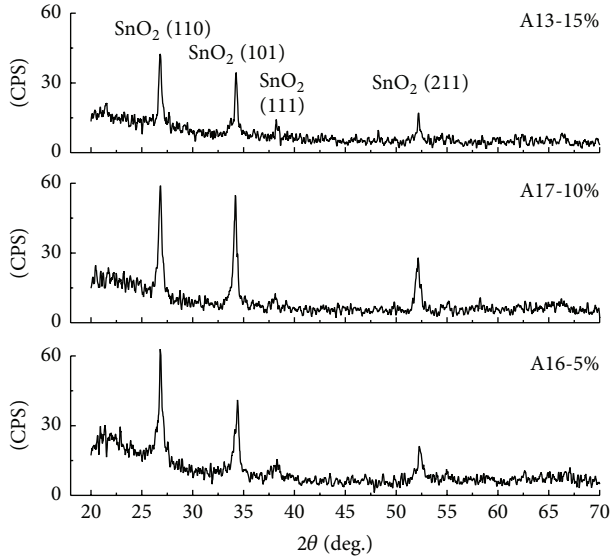

Figure 6: The X-ray diffraction patterns of (a) 5%, (b) 10%, and (c) 15% ATO films annealed at 500°C for 2 h after being deposited at room temperature.

Figure 6 illustrates the XRD patterns of the as-deposited samples annealed for 2 h at 500°C with various Sb_2O_3-doping percentages. The 5% and 10% ATO films do not show the presence of a Sn_2O_3 phase as 15% ATO films. Thus, the number of Sb^{3+} ions substituting for Sn^{4+} ions was enough to supply the energy required for the oxidation process of Sn_2O_3 transforming to SnO_2 at minimum doping percentages of 5 wt% Sb_2O_3.

3.2. Electrical Properties of ATO. As seen in Table 1, all of the SnO_2 films deposited at various temperatures including sample S6 exhibit n-type conductivity due to oxygen vacancies and tin interstitials. This result has been also given in [38, 39] at a certain deposition temperature. On the other hand, the samples A5 and A6 of 15% ATO films showed p-type conductivity. Clearly, antimony atoms substituted for tin sites at 500°C temperature and this substitution was recorded at the deposition temperatures of 600 and 700°C as mentioned in [34]. In particular, the carrier concentration increased from 10^{15} to 10^{16}, and the carrier mobility decreased from 19.3 to 3.49 after annealing at 600°C following the direct deposition at 500°C. The decrease in the carrier mobility is attributed to the increase in ionized acceptors as mentioned in [24]. Therefore, it is obvious that the annealing method plays an important role in the electrical properties of the ATO films.

As seen in Table 2, the SnO_2 and ATO films were nonconductive at room temperature and were n-type at 200°C; however, the ATO films had much lower resistivities compared to the SnO_2 films. This effect might also be explained as follows: creating donors such as oxygen vacancies, tin interstitials as mentioned in [23, 25, 28, 31, 32, 38, 40], and unintentional hydrogen dopants as in agreement with previous theoretical and experimental studies [41–44] compensate by the Sn^{2+} acceptors [29, 32] at room temperature, leading to nonconductive SnO_2 and ATO films, while Sb appear as a result of the dissociation of Sb_2O_3 at 200°C, which supplies more negative carriers for the ATO films leading to a resistivity of the ATO films lower than that of the SnO_2 film. This dissociation of Sb_2O_3 shows clearly at optical properties (Figure 10). The SnO_2 films annealed at a temperature in the range of 300–500°C are nonconductive because Sn^{+2} is oxidized to Sn^{4+} [45], the oxygen vacancies are filled with the oxygen present in the ambient air, and unintentional hydrogen donors are driven out of films [43, 46]. The 15% ATO films annealed at 300°C are n-type, whereas, in the range of 400–600°C, the 15% ATO films show p-type conductivity because the Sb^{3+} substitutes for Sn^{4+}. Several authors have also observed this phenomenon that the conduction type of In-Ga co- [26], Sb- [24], Ga- [27], Zn- [25, 28], or In-doped SnO_2 [23] changed from n-type to p-type at a certain annealing temperature. The SnO_2 films annealed at 550°C are p-type, which is attributed to the dissociation from SnO_2 to Sn_2O_3 being in agreement with results of structure analyzing. However, the resistivity of SnO_2 film is much higher than that of the 15% ATO film annealed at 550°C. It was found that hole carriers were formed by Sb^{3+} replacing Sn^{4+} rather than by Sn^{3+} replacing Sn^{4+}. Indeed, the hole concentration of the SnO_2 films decreased at 550°C because the Sn_2O_3 phases were oxidized and this also increased the mobility. Contrarily, the hole concentration of the 15% ATO films first increased with increases in the annealing temperature, and the highest hole concentration was obtained after annealing at 550°C for 1 h. As the annealing temperature was further increasing, the hole concentration value started to decrease because of disappearing of acceptor Sn^{3+} and native donors being able to appear. The 15% ATO films annealed at 550°C for 1 h had low resistivities (0.83 Ω·cm) and high hole concentrations (4.4×10^{18} cm^{-3}). However, in the following section, we increased the annealing time of the ATO films to confirm the effect of the Sn^{3+} on the electrical properties.

Table 1: The results of the Hall measurements of SnO_2 and 15% ATO films that were directly deposited at different temperatures.

T (°C)	SnO_2					15% ATO				
	Sample	ρ (Ω·cm)	μ ($cm^2V^{-1}s^{-1}$)	N (cm^{-3})	Type	Sample	ρ (Ω·cm)	μ ($cm^2V^{-1}s^{-1}$)	N (cm^{-3})	Type
RT	S1	∞				A1	∞			
200	S2	1.0	1.39	-4.5×10^{18}	n	A2	43.8	0.02	-7.1×10^{18}	n
300	S3	3.5	0.51	-3.4×10^{18}	n	A3	1.2	0.44	-1.2×10^{19}	n
400	S4	0.5	2.21	-5.2×10^{18}	n	A4	1.7	2.79	-1.3×10^{18}	n
500	S5	0.05	3.90	-3.6×10^{19}	n	A5	43.6	19.30	7.4×10^{15}	p
500 annealed 600	S6	2.81	1.27	-1.75×10^{18}	n	A6	26.1	3.49	6.9×10^{16}	p

Table 2: The results of the Hall measurements of SnO_2 and ATO films annealed at different temperatures after being deposited at room temperature.

T (°C)	SnO_2					ATO				
	Sample	ρ (Ω·cm)	μ ($cm^2V^{-1}s^{-1}$)	N (cm^{-3})	Type	Sample	ρ (Ω·cm)	μ ($cm^2V^{-1}s^{-1}$)	N (cm^{-3})	Type
RT	S1	∞				A1	∞			
200	S7	17.11	2.51	-1.5×10^{17}	n	A7	4.50	0.65	-2.1×10^{18}	n
300	S8	∞				A8	12.80	2.61	-1.8×10^{17}	n
400	S9	∞				A9	71.80	0.81	1.1×10^{17}	p
500	S10	∞				A10	30.60	1.72	1.2×10^{17}	p
550	S11	278	1.59	1.4×10^{16}	p	A11	0.83	1.73	4.4×10^{18}	p
600	S12	153	3.10	1.3×10^{16}	p	A12	4.20	2.90	5.1×10^{17}	p

Table 3: The results of the Hall measurements of 15% ATO films annealed at different temperatures for 1 h and 2 h after being deposited at room temperature.

T (°C)	ATO films annealed for 1 h			ATO films annealed for 2 h				
	ρ (Ω·cm)	μ ($cm^2V^{-1}s^{-1}$)	N (cm^{-3})	Sample	ρ (Ω·cm)	μ ($cm^2V^{-1}s^{-1}$)	N (cm^{-3})	Type
500	30.60	1.72	1.2×10^{17}	A13	0.78	2.48	3.2×10^{18}	p
550	0.83	1.73	4.4×10^{18}	A14	1.00	1.13	5.5×10^{18}	p
600	4.20	2.90	5.1×10^{17}	A15	2.13	1.13	2.6×10^{18}	p

Table 4: The results of the Hall measurements of (a) 5% ATO, (b) 10% ATO, and (c) 15% ATO films annealed at 500°C after being deposited at room temperature.

Sample	Sb_2O_3 concentration (wt%)	ρ (Ω·cm)	μ ($cm^2V^{-1}s^{-1}$)	N (cm^{-3})	Type
A16	5	36.80	0.18	9.5×10^{17}	p
A17	10	0.55	0.54	1.2×10^{19}	p
A13	15	0.78	2.48	3.2×10^{18}	p

As we see in Table 3, the resistivity increased slightly due to decreasing hole mobility as samples were annealed at 550°C for 2 h compared to 1 h regardless existence of Sn_2O_3 phase in films. Contrarily, the resistivity decreases as samples were annealed at 500°C for 2 h compared to 1 h without existing Sn_2O_3 phase in films. In conclusion, the contribution of the hole concentration is primarily from the substitution of Sn^{4+} by Sb^{3+}, while the contribution from Sn^{3+} is minor. The other issue, we determined the effect of the doping percentage on the electrical properties.

As seen in Table 4, the resistance first decreases with increasing Sb concentration, and the lowest resistance is obtained at a doping concentration of 10 wt%. The 10% ATO films had the lowest resistivity (0.55 Ω·cm) and the highest hole concentration (1.2×10^{19} cm^{-3}). As the wt% Sb_2O_3 was further increased, the resistance value started to increase. Our present observations suggest that beyond a certain doping concentration, the doping atoms do not occupy the lattice sites but instead produce some types of defects.

3.3. Optical Properties. At room temperature, both SnO_2 and ATO films have absorption edge in visible light at 431 nm (2.87 eV) for SnO_2 films and 350 nm for ATO films; this indicates existence of defect level Sn^{2+} [47] which served as an acceptor; electron at acceptor energy level Sn^{2+} absorbed light energy so that it transited to conduction band (Figure 7); this transited energy differ from exciton transited energy. At 200°C, the absorption edge significantly shifts to the shorter wavelength side; at above 200°C, this shifts was slight. This is due to acceptor Sn^{2+} transform to Sn^{4+}, particular at 500°C band gap energy is exciton absorbed energy (Figures 7 and 8).

Figure 9 presents the transmittance spectra of SnO_2 films with different annealing temperatures. At room temperature, the transmittance spectra of SnO_2 films were taken from

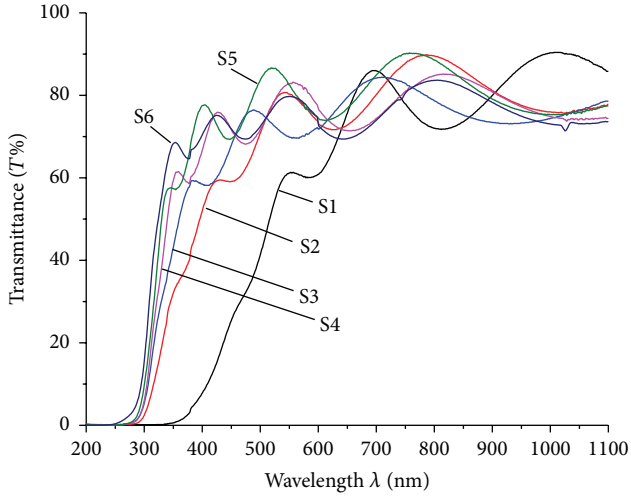

Figure 7: The UV-visible spectra of SnO_2 films prepared at different annealing temperatures.

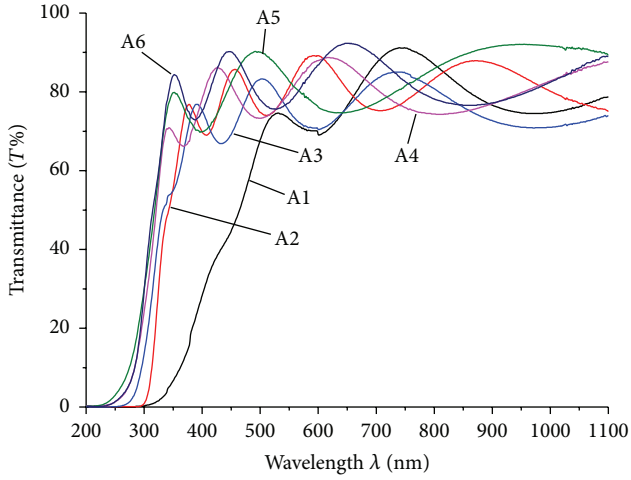

Figure 8: The UV-visible spectra of 15% ATO films prepared at different annealing temperatures.

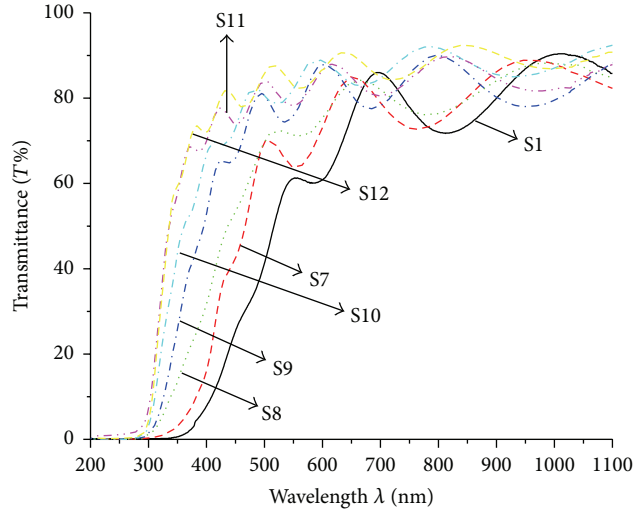

Figure 9: The UV-visible spectra of SnO_2 films prepared at different annealing temperatures after being deposited at room temperature.

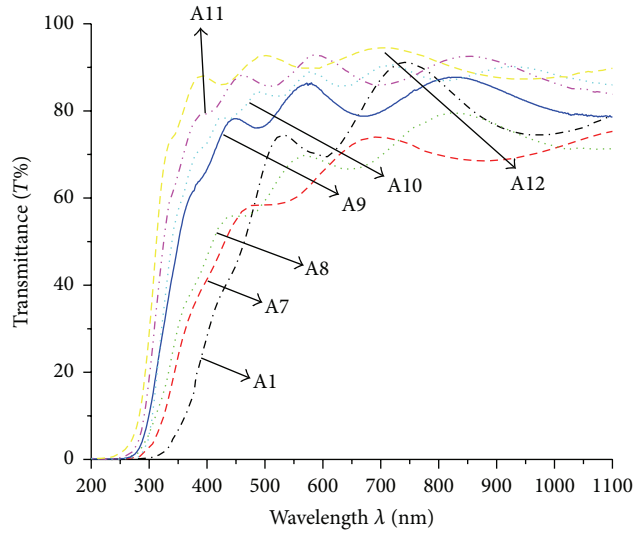

Figure 10: The UV-visible spectra of 15% ATO films prepared at different annealing temperatures after being deposited at room temperature.

Figure 7. Above 200°C, acceptor Sn^{2+} were supplied energy to transform to Sn^{4+} so that the average transmittance in the visible region increased gradually above 80%; furthermore, the absorption edge gradually shifts to the shorter wavelength side. Meanwhile, Figure 10 shows that the ATO films have lower average transmittances compared to the SnO_2 films at temperatures below 400°C, which indicates the decomposition of Sb_2O_3 to form Sb which has discrete distribution in films, and this causes a decrease in the transmittance due to their absorption. It does not occur at ATO films deposited at 200°C. The transmittance in the visible region increased to 80% at 500°C. This effect occurs because, with increasing temperature, the doping Sb enters the film from interstitial sites and substitutes into other positions.

Figure 11 presents the spectral transmittance of 5%, 10%, and 15% ATO films with the same thickness annealed at 500°C for 2 h. The average transmissions of the 5%, 10%, and 15% ATO films in the visible region (300–800 nm) were approximately 80%. All these results are promising for diverse applications in the field of transparent electronics.

3.4. XPS Analysis. Figures 12 and 13 show that the results of the XPS spectra of the O 1s and the Sn core-level of the ATO films with different Sb concentrations were annealed at 500°C for 2 h after being deposited at room temperature and SnO_2 films were annealed at 550°C for 1 h after being deposited at room temperature. All peak positions were corrected for surface charge by the C 1s peak at 284.5 eV. The O 1s spectrum can be deconvoluted into three peaks for the SnO_2 (530, 531.5, and 532.5 eV) using XPSEAK41 software, and the profile of each peak was taken as a Lorentzian-Gaussian mixed function, respectively. For SnO_2 films, deconvolutions contained the 3 peaks of O 1s at 530, 531, and 532.5 eV. Two

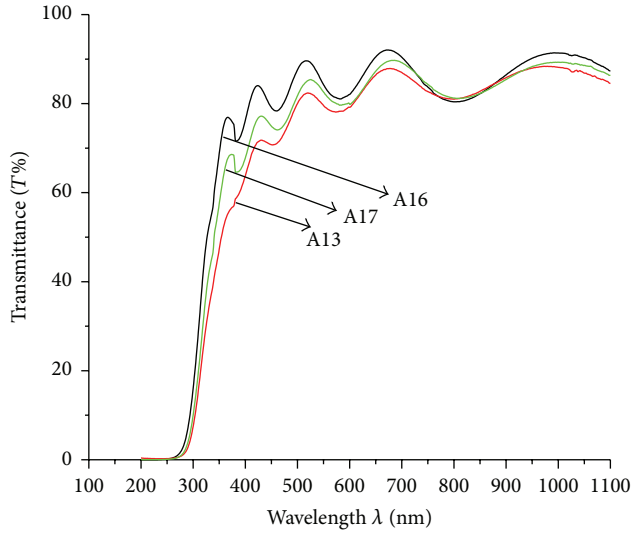

Figure 11: The UV-visible spectra of 5%, 10%, and 15% ATO films annealed at 500°C for 2 h after being deposited at room temperature.

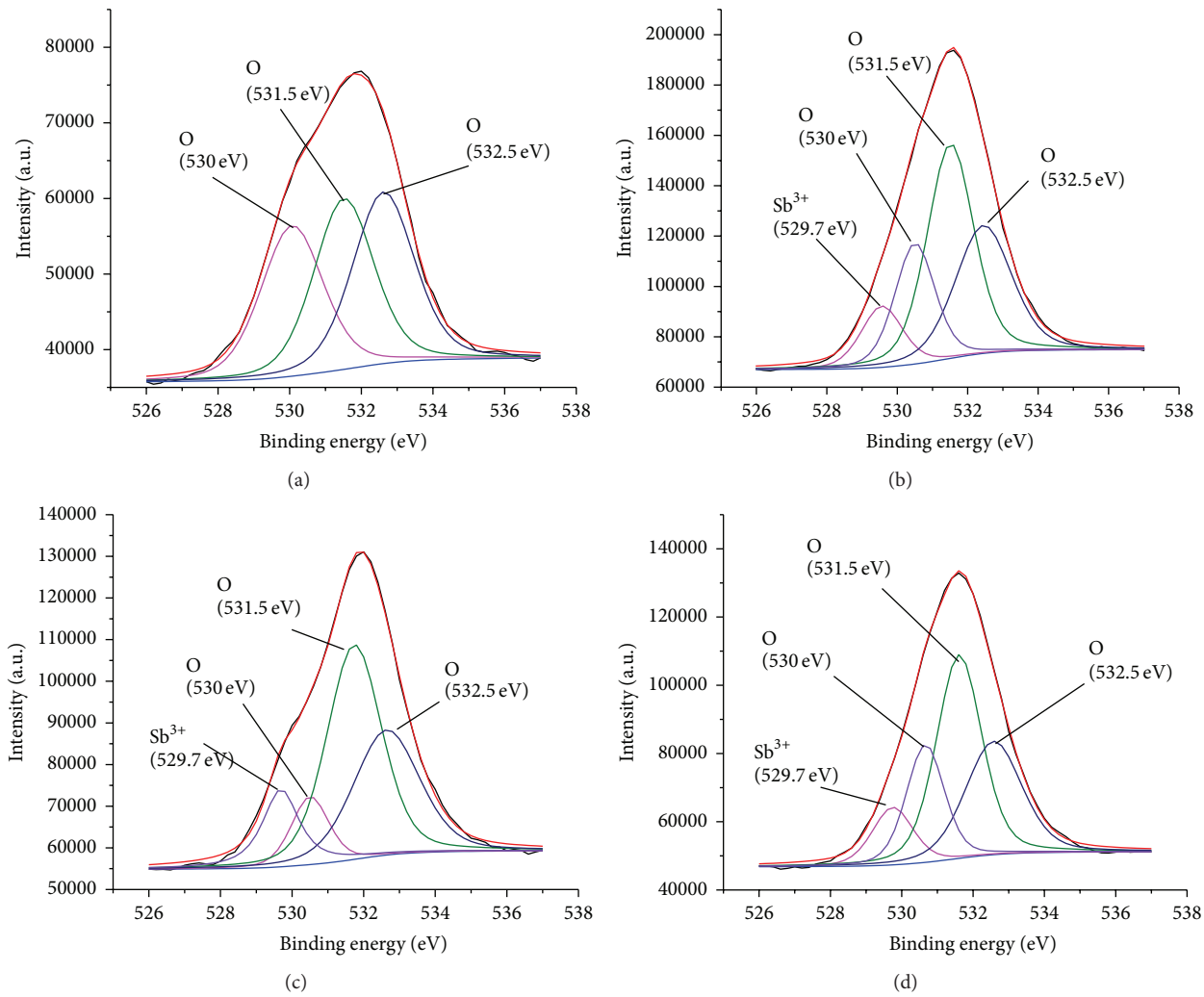

Figure 12: The O 1S XPS spectra (open circles) and deconvoluted results (line) of (a) SnO_2, (b) 5%, (c) 10%, and (d) 15% ATO films annealed at 500°C for 2 h after being deposited at room temperature.

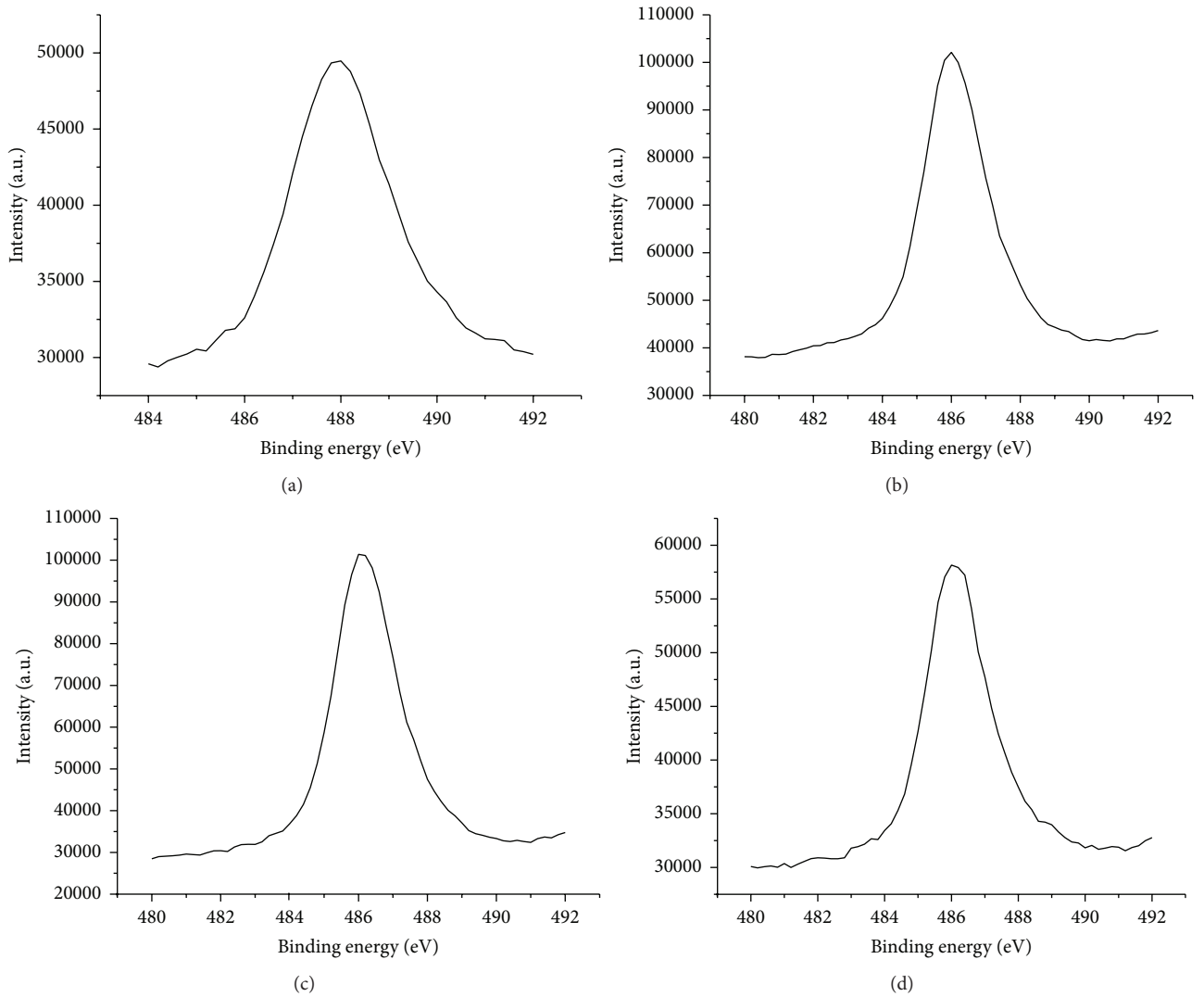

Figure 13: The $Sn3d_{5/2}$ XPS spectra of (a) SnO_2, (b) 5%, (c) 10%, and (d) 15% ATO films annealed at 500°C for 2 h after being deposited at room temperature.

Table 5: XPS analyses of the surface of the SnO_2 and ATO films.

Sample	% $O_{531.5}$	% Sn	% O_{530}	% Sb	$[O_{530} + O_{531.5}]/2[Sn] + 1.5[Sb]$
S11 (SnO_2)	26.55	25.94	47.50	—	1.427
A16 (5% ATO)	36.84	36.58	17.59	8.97	0.628
A17 (10% ATO)	24.77	59.34	5.09	10.79	0.221
A13 (15% ATO)	41.13	27.86	19.63	10.37	0.866

peaks at 530 and 531.5 eV can be attributed to O^{2-} ions in the rutile structure of the Sn^{4+} ion array [48] and the O^{2-} ions in oxygen-deficient regions [49]. The peak at 532.5 eV is assigned to the adsorbed oxygen species [50]. The above deconvolutions of all ATO films contained the 3 peaks of O 1s and 1 peak at 529.5 eV due to the contribution of the Sb^{3+} species [50]. This peak was attributed to the substitution of Sn^{4+} by Sb^{3+}. It showed clearly that the peak for the Sn $3d_{3/2}$ of ATO films shifted to a lower binding energy compared to that of SnO_2 films. The atomic percentages and compositional ratios of all the samples were calculated by the ratio between the integrated areas of $O_{531.5}$ and O_{530} peaks and the integrated areas of the 2Sn and 1.5Sb peaks, and the results are listed in Table 5. In ideal stoichiometric SnO_2 films, the $[O_{530} + O_{531.5}]/(2[Sn] + 1.5[Sb])$ ratio must have been 1, but the results in Table 5 give 1.427, indicating that valence state of Sn was not 4 perfectly and including lower valence state such as Sn^{3+}. These results were in agreement with the existence of acceptor Sn^{3+} discussed in structure and electrical properties (3.1 and 3.2). For ATO, this ratio varied

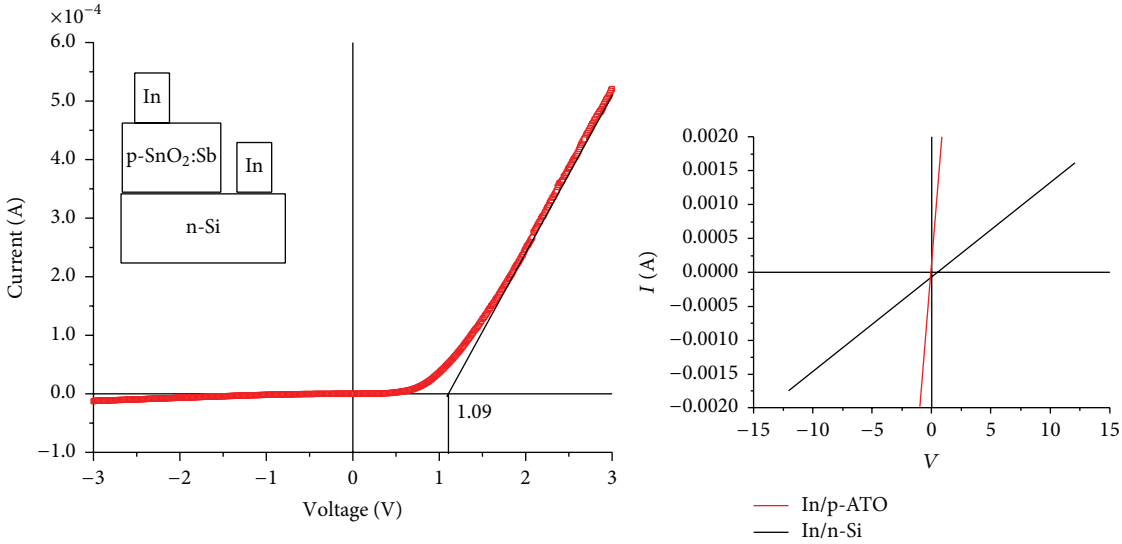

FIGURE 14: The *I-V* characteristics of the p-type ATO/n-Si heterojunction. The insets show a schematic diagram of the p-n heterojunction (upper left) and the *I-V* characteristics of In contacts on the p-type and n-type (lower right).

from 0.221–0.866, which indicates the existence of numerous oxygen deficiencies (the ratio was 1 for stoichiometric ATO films). The oxygen deficiencies prove substitution of Sn^{4+} by Sb^{3+}. Moreover, the O 1s peak of 10 wt% Sb_2O_3 was asymmetric proving the highest substitution of Sn^{4+} by Sb^{3+}, resulting in the highest concentration of holes (relative to the lowest ratio).

3.5. Properties of p-Type ATO/n-Type Si Heterojunction. To confirm the fabrication of p-type conductive ATO films, a p-type 10% ATO was selected as a p-type layer due to its high hole concentration of 1.2×10^{19}, and they were fabricated on an n-type Si substrate. The current-voltage characteristics of the p-type ATO/n-type Si structure are plotted in Figure 14. Indium electrodes were placed both on the p-type and the n-type layers, as shown in the upper left inset. The lower right inset shows the *I-V* curves for a pair of In contacts on the p-type and n-type material layers. The linear *I-V* characteristics indicate good ohmic contact behavior. It is found that the *I-V* curve of the heterojunction p-type ATO/n-type Si is nonlinear. This characteristic clearly indicates the formation of p-n junction at the interface. Figure 14 also shows a forward turn-on voltage of 1.09 V.

4. Conclusions

In summary, p-type transparent conducting ATO films were prepared by DC magnetron sputtering. It was found that an annealing temperature of 500°C for 2 h was necessary for high p-type conductivity. The best electrical properties of the film were obtained from 10 wt% Sb_2O_3-doped SnO_2 target with a resistivity, hole concentration, and Hall mobility of 0.55 Ω·cm, 1.2×10^{19} cm^{-3}, and 0.54 $cm^2V^{-1}s^{-1}$, respectively. The XPS analysis indicated that Sb exists in the form of Sb^{3+} in the film and acts as an acceptor. The ATO films show polycrystalline tetragonal rutile structure and their average transmittance is above 80% in the visible light range. The p-n heterojunction diode composed of p-ATO/n-Si exhibits good *I-V* characteristics, thereby, demonstrating that a p-type ATO film and its fabrication technology might have a promising future in practical applications.

Competing Interests

The authors declare that there are no competing interests regarding the publication of this paper.

Acknowledgments

This research was funded by the Vietnam National University (VNU-HCM), Ho Chi Minh City, under Grant no. C2014-18-27.

References

[1] V. G. Kytin, V. A. Kulbachinskii, O. V. Reukova et al., "Conducting properties of In_2O_3:Sn thin films at low temperatures," *Applied Physics A*, vol. 114, no. 3, pp. 957–964, 2014.

[2] V. Musat, B. Teixeira, E. Fortunato, R. C. C. Monteiro, and P. Vilarinho, "Al-doped ZnO thin films by sol–gel method," *Surface and Coatings Technology*, vol. 180-181, pp. 659–662, 2004.

[3] M. V. Castro and C. J. Tavares, "Dependence of Ga-doped ZnO thin film properties on different sputtering process parameters: substrate temperature, sputtering pressure and bias voltage," *Thin Solid Films*, vol. 586, pp. 13–21, 2015.

[4] T. Tsuchiya, T. Nakajima, and K. Shinoda, "Electrical properties of Sb-doped epitaxial SnO_2 thin films prepared using excimer-laser-assisted metal-organic deposition," *Applied Physics B*, vol. 113, no. 3, pp. 333–338, 2013.

[5] T. Maruyama and K. Tabata, "Fluorine doped tin dioxide thin films prepared by chemical vapor deposition," *Journal of Applied Physics*, vol. 68, no. 8, pp. 4282–4285, 1990.

[6] M. K. Jayaraj, A. D. Draeseke, J. Tate, and A. W. Sleight, "p-type transparent thin films of $CuY_{1-x}Ca_xO_2$," *Thin Solid Films*, vol. 397, no. 1-2, pp. 244–248, 2001.

[7] N. Duan, A. W. Sleight, M. K. Jayaraj, and J. Tate, "Transparent p-type conducting $CuScO_{2+x}$ films," *Applied Physics Letters*, vol. 77, no. 9, article 1325, 2000.

[8] R. Nagarajan, A. D. Draeseke, A. W. Sleight, and J. Tate, "*p*-type conductivity in $CuCr_{1-x}Mg_xO_2$ films and powders," *Journal of Applied Physics*, vol. 89, no. 12, pp. 8022–8025, 2001.

[9] R. Nagarajan, N. Duan, M. K. Jayaraj et al., "p-Type conductivity in the delafossite structure," *International Journal of Inorganic Materials*, vol. 3, no. 3, pp. 265–270, 2001.

[10] F. Mao, T. Nyberg, T. Thersleff, A. M. Andersson, and U. Jansson, "Combinatorial magnetron sputtering of $AgFeO_2$ thin films with the delafossite structure," *Materials & Design*, vol. 91, pp. 132–142, 2016.

[11] Y. Liu, S. Pollaor, and Y. Wu, "Electrohydrodynamic processing of p-Type transparent conducting oxides," *Journal of Nanomaterials*, vol. 2015, Article ID 423157, 14 pages, 2015.

[12] A. Janotti and C. G. Van de Walle, "Native point defects in ZnO," *Physical Review B*, vol. 76, no. 16, Article ID 165202, 2007.

[13] S. B. Zhang, S.-H. Wei, and A. Zunger, "Intrinsic *n*-type versus *p*-type doping asymmetry and the defect physics of ZnO," *Physical Review B*, vol. 63, no. 7, Article ID 075205, 7 pages, 2001.

[14] A. Kobayashi, O. F. Sankey, and J. D. Dow, "Deep energy levels of defects in the wurtzite semiconductors AIN, CdS, CdSe, ZnS, and ZnO," *Physical Review B*, vol. 28, no. 2, pp. 946–956, 1983.

[15] B. Ding and J. Yu, *Electrospun Nanofibers for Energy and Environmental Applications*, Nanostructure Science and Technology, Springer, New York, NY, USA, 2014.

[16] S. S. Pan, C. Ye, X. M. Teng, H. T. Fan, and G. H. Li, "p-type conduction in nitrogen-doped SnO_2 films grown by thermal processing of tin nitride films," *Applied Physics A*, vol. 85, pp. 21–24, 2006.

[17] T. Minami, H. Sonohara, S. Takata, and H. Sato, "Highly transparent and conductive zinc-stannate thin films prepared by RF magnetron sputtering," *Japanese Journal of Applied Physics*, vol. 33, pp. L1693–L1696, 1994.

[18] R. K. Nath and S. S. Nath, "Tin dioxide thin-film-based ethanol sensor prepared by spray pyrolysis," *Sensors and Materials*, vol. 21, no. 2, pp. 95–104, 2009.

[19] E. Çetinörgü, C. Gümüs, S. Goldsmith, and F. Mansur, "Optical and structural characteristics of tin oxide thin films deposited by filtered vacuum arc and spray pyrolysis," *Physica Status Solidi A: Applications and Materials Science*, vol. 204, no. 10, pp. 3278–3285, 2007.

[20] K. Ravichandran and K. Thirumurugan, "Type inversion and certain physical properties of spray pyrolysed SnO_2:Al films for novel transparent electronics applications," *Journal of Materials Science and Technology*, vol. 30, no. 2, pp. 97–102, 2014.

[21] K.-Y. Park, G.-W. Kim, Y.-J. Seo et al., "Effect of annealing temperature on properties of p-type conducting $Al/SnO_2/Al$ multilayer thin films deposited by sputtering," *Journal of Ceramic Processing Research*, vol. 13, no. 2, pp. s385–s389, 2012.

[22] T. Yang, X. Qin, H.-H. Wang et al., "Preparation and application in p–n homojunction diode of p-type transparent conducting Ga-doped SnO_2 thin films," *Thin Solid Films*, vol. 518, no. 19, pp. 5542–5545, 2010.

[23] Z. Ji, Z. He, Y. Song, K. Liu, and Z. Z. Ye, "Fabrication and characterization of indium-doped p-type SnO_2 thin films," *Journal of Crystal Growth*, vol. 259, no. 3, pp. 282–285, 2003.

[24] J. Ni, X. Zhao, X. Zheng, J. Zhao, and B. Liu, "Electrical, structural, photoluminescence and optical properties of p-type conducting, antimony-doped SnO_2 thin films," *Acta Materialia*, vol. 57, no. 1, pp. 278–285, 2009.

[25] J. M. Ni, X. J. Zhao, and J. Zhao, "Structural, electrical and optical properties of p-Type transparent conducting SnO_2:Zn film," *Journal of Inorganic and Organometallic Polymers and Materials*, vol. 22, no. 1, pp. 21–26, 2012.

[26] Q. Mao, Z. Ji, and L. Zhao, "Mobility enhancement of p-type SnO_2 by In–Ga co-doping," *Physica Status Solidi (B)*, vol. 247, no. 2, pp. 299–302, 2010.

[27] F. Finanda, Damisih, H. C. Ma, and H. Y. Lee, "Characteristics of p-type gallium tin oxide (GTO) thin films prepared by RF magnetron sputtering," *Journal of Ceramic Processing Research*, vol. 13, no. 2, pp. s181–s185, 2012.

[28] J. Ni, X. Zhao, and J. Zhao, "P-type transparent conducting SnO_2:Zn film derived from thermal diffusion of $Zn/SnO_2/Zn$ multilayer thin films," *Surface & Coatings Technology*, vol. 206, no. 21, pp. 4356–4361, 2012.

[29] S. S. Pan, G. H. Li, L. B. Wang et al., "Atomic nitrogen doping and p-type conduction in SnO_2," *Applied Physics Letters*, vol. 95, no. 22, Article ID 222112, 2009.

[30] S. S. Pan, S. Wang, Y. X. Zhang et al., "P-type conduction in nitrogen-doped SnO_2 films grown by thermal processing of tin nitride films," *Applied Physics A*, vol. 109, no. 2, pp. 267–271, 2012.

[31] S. S. Lekshmy and K. Joy, "Structural and optoelectronic properties of indium doped SnO_2 thin films deposited by sol gel technique," *Journal of Materials Science: Materials in Electronics*, vol. 25, no. 4, pp. 1664–1672, 2014.

[32] C.-Y. Tsay and S.-C. Liang, "Fabrication of p-type conductivity in SnO_2 thin films through Ga doping," *Journal of Alloys and Compounds*, vol. 622, pp. 644–650, 2015.

[33] M.-M. Bagheri-Mohagheghi and M. Shokooh-Saremi, "Electrical, optical and structural properties of Li-doped SnO_2 transparent conducting films deposited by the spray pyrolysis technique: a carrier-type conversion study," *Semiconductor Science and Technology*, vol. 19, no. 6, pp. 764–769, 2004.

[34] S. Yu, W. Zhang, L. Li, D. Xu, H. Dong, and Y. Jin, "Fabrication of p-type SnO_2 films via pulsed laser deposition method by using Sb as dopant," *Applied Surface Science*, vol. 286, pp. 417–420, 2013.

[35] S. W. Lee, Y.-W. Kim, and H. Chen, "Electrical properties of Ta-doped SnO_2 thin films prepared by the metal-organic chemical-vapor deposition method," *Applied Physics Letters*, vol. 78, no. 3, pp. 350–352, 2001.

[36] J. Montero, C. Guillén, C. G. Granqvist, J. Herrero, and G. A. Niklasson, "Preferential orientation and surface oxidation control in reactively sputter deposited nanocrystalline SnO_2:Sb films: electrochemical and optical results," *ECS Journal of Solid State Science and Technology*, vol. 3, no. 11, pp. N151–N153, 2014.

[37] A. Rabis, D. Kramer, E. Fabbri, M. Worsdale, R. Kötz, and T. J. Schmidt, "Catalyzed SnO_2 thin films: theoretical and experimental insights into fabrication and electrocatalytic properties," *Journal of Physical Chemistry C*, vol. 118, no. 21, pp. 11292–11302, 2014.

[38] Y. Porte, R. Maller, H. Faber, H. N. AlShareef, T. D. Anthopoulos, and M. A. McLachlan, "Exploring and controlling intrinsic

defect formation in SnO_2 thin films," *Journal of Materials Chemistry C*, vol. 4, no. 4, pp. 758–765, 2016.

[39] J.-H. Lee, G.-E. Jang, D.-H. Yoon, and S.-H. Son, "Effect of deposition temperature on electro-optical properties of SnO_2 thin films fabricated by a PECVD method," *Journal of Ceramic Processing Research*, vol. 8, no. 1, pp. 59–63, 2007.

[40] Y. Huang, Z. Ji, and C. Chen, "Preparation and characterization of p-type transparent conducting tin-gallium oxide films," *Applied Surface Science*, vol. 253, no. 11, pp. 4819–4822, 2007.

[41] Ç. Kılıç and A. Zunger, "n-type doping of oxides by hydrogen," *Applied Physics Letters*, vol. 81, no. 1, article 73, 2002.

[42] D. O. Scanlon and G. W. Watson, "On the possibility of p-type SnO_2," *Journal of Materials Chemistry*, vol. 22, no. 48, pp. 25236–25245, 2012.

[43] J. B. Varley, A. Janotti, A. K. Singh, and C. G. Van De Walle, "Hydrogen interactions with acceptor impurities in SnO_2: first-principles calculations," *Physical Review B*, vol. 79, no. 24, Article ID 245206, 2009.

[44] N. M. Johnson, "Mechanism for hydrogen compensation of shallow-acceptor impurities in single-crystal silicon," *Physical Review B*, vol. 31, no. 8, pp. 5525–5528, 1985.

[45] K. Nomura, "Magnetic properties and oxygen defects of dilute metal doped tin oxide based semiconductor," *Croatica Chemica Acta*, vol. 88, no. 4, pp. 579–590, 2015.

[46] X. H. Huang, C. B. Tay, Z. Y. Zhan et al., "Universal photoluminescence evolution of solution-grown ZnO nanorods with annealing: important role of hydrogen donor," *CrystEngComm*, vol. 13, no. 23, pp. 7032–7036, 2011.

[47] E. Fortunato, R. Barros, P. Barquinha et al., "Transparent p-type SnO_x thin film transistors produced by reactive rf magnetron sputtering followed by low temperature annealing," *Applied Physics Letters*, vol. 97, no. 5, Article ID 052105, 2010.

[48] D. J. Shuttleworth, "Preparation of metal-polymer dispersions by plasma techniques. An ESCA investigation," *The Journal of Physical Chemistry*, vol. 84, no. 12, pp. 1629–1634, 1980.

[49] A. Chen, K. Zhu, H. Zhong, Q. Shao, and G. Ge, "A new investigation of oxygen flow influence on ITO thin films by magnetron sputtering," *Solar Energy Materials & Solar Cells*, vol. 120, pp. 157–162, 2014.

[50] J. M. Wu, "A room temperature ethanol sensor made from p-type Sb-doped SnO_2 nanowires," *Nanotechnology*, vol. 21, no. 23, Article ID 235501, 2010.